STRUCTURE TENSOR BASED SYNTHESIS OF DIRECTIONAL TEXTURES FOR VIRTUAL MATERIAL DESIGN

Adib Akl[1,2], Charles Yaacoub[2], Marc Donias[1], Jean-Pierre Da Costa[1], Christian Germain[1]

[1]Bordeaux University, IMS Lab, UMR CNRS 5218, France
[2]Faculty of Engineering, Holy Spirit University of Kaslik (USEK), Jounieh, Lebanon

ABSTRACT

Exemplar-based texture synthesis schemes are promising for virtual material design. They provide impressive results in many cases, but fail in difficult situations with large and multi-scale patterns, or with long range directional variations. Since a prior synthesis of a geometric layer may help in the synthesis of the texture layer, a two-stage structure/texture synthesis algorithm is proposed. At the first stage, a structure tensor map carrying information about the local orientation is synthesized from the exemplar's data, and at the second stage, the synthesized tensor field is used to constrain the synthesis of the texture. Results show that the proposed approach not only yields better synthesized textures, but also successfully synthesizes the output texture in many situations where traditional algorithms fail to reproduce the exemplar's patterns, which paves the way towards the synthesis of accurately large and multi-scale patterns as it is the case for pyrolytic carbon samples showing laminar structures observed by Transmission Electronic Microscopy.

Index Terms— Non Parametric Texture Synthesis, Structure Tensor, Exemplar Based Synthesis, Virtual Material, Pyrolytic Carbon Simulation.

1. INTRODUCTION

Natural textures can be efficiently modeled and reproduced using image techniques. In the past decades, several parametric and non-parametric algorithms have been proposed for the analysis and synthesis of 2D and 3D textures [1-7]. They have shown to successfully deal with a large panel of textures, including stochastic and structured textures, in many application domains such as image extrapolation, texture inpainting and virtual material simulation. For instance, Portilla and Simoncelli [2] use an over complete complex wavelet transform in order to parameterize the model by a set of statistics corresponding to basic functions at adjacent locations, orientations and scales. The 2D texture synthesis algorithm proposed by Wei and Levoy in [3] relies on the assumptions of a Markov Random Field, modeling the texture as a realization of a local and stationary random process. The algorithm starts from a sample texture and an output image initialized by a white random noise [4]. The texture is synthesized in a scan-line order; for each output pixel, the neighborhood of the current pixel is captured and the most similar neighborhood is searched for in the exemplar based on the Euclidian distance, then the corresponding pixel is copied to the target position in the output texture. Paget and Longstaff [5] propose a Markov Random Field texture modeling method based on non-parametric estimation of the local conditional probability density function. It mathematically captures the visual characteristics of a texture into a unique statistical model that describes the interactions between pixel values. Kwatra et al. [6] propose a synthesis algorithm based on copying patch regions from the sample to the output and then stitching them together along optimal seams. They use a graph cut technique to determine the patch region without choosing its size a-priori, in contrast to many other existing methods.

Various extensions to 3D, i.e. solid texture synthesis, have also been proposed. Among such extensions, the non-parametric approach of Kopf et al. [7] integrates histogram matching to help the global statistics of the synthesized solid converge towards those of the exemplar. Other 2D/3D extensions of either parametric [8] or non-parametric approaches [9] have also shown to be relevant in many cases including virtual material design [10, 11].

For the synthesis of structured anisotropic textures, such as those of pyrolytic carbon materials observed at the nanometric scale, most of existing approaches tend to produce more regular textures than the exemplar, dealing badly with long range orientation variations [1], as shown in Fig.5. As a corollary, they are hardly able to synthesize textures with non stationarities such as undulating or circular laminar structures. However, it was mentioned in [12] that prior synthesis of a geometric layer may help in the synthesis of the texture layer. In the case of locally anisotropic textures, a two-step synthesis approach could consist in first producing a structure layer from the analysis of the original exemplar, and the resulting synthetic structure would then constrain the synthesis of the texture itself.

In this paper, we analyze and represent the structure layer through the structure tensor field which carries information about the local orientation and degree of anisotropy [13]. The synthesis of the structure layer consists in synthesizing the texture tensor field. The non-parametric Wei and Levoy (WL) algorithm [3], which usually operates on scalar data, is adapted to the specificities of tensor-valued images and used to synthesize a tensor field similar to the exemplar's. Relevant multi-scale decompositions and tensor metrics

are used for this purpose. Once the structure layer is available, it is used to drive the synthesis of the texture layer. The WL approach is also used as the basis for the texture synthesis algorithm, since it can easily incorporate additional constraints such as the local anisotropy provided by the structure tensor field.

The remainder of this paper is organized as follows. The tensor field synthesis algorithm and the dissimilarity metrics are described in Section 2. Section 3 presents the proposed texture synthesis algorithm constrained by the synthesized structure tensor field. Practical results and application to a composite material sample are discussed in Section 4, and conclusions are drawn in Section 5.

2. TEXTURE TENSOR FIELD SYNTHESIS

The structure tensor S of an image I is defined in [14] as the covariance matrix of the first partial derivatives of I, and built from previously estimated gradient fields $\nabla I = [I_x, I_y]$, as follows:

$$I_x = I * G_x, \quad I_y = I * G_y, \tag{1}$$

where G_x and G_y are Gaussian derivatives Kernel, and the symbol (*) denotes convolution.

At a point *(x, y)*, the structure tensor *S(x, y)* is symmetric and can be written as:

$$S(x,y) = \begin{bmatrix} S_{xx}(x,y) & S_{xy}(x,y) \\ S_{xy}(x,y) & S_{yy}(x,y) \end{bmatrix}; \tag{2}$$

the tensor components S_{xx}, S_{xy}, and S_{yy} are given by:

$$S_{xx} = W * (I_x I_x); \; S_{xy} = W * (I_x I_y); \; S_{yy} = W * (I_y I_y), \tag{3}$$

where W is a weighting function - usually Gaussian - used for gradient field smoothing.

In 2D, the structure tensor can be interpreted as an ellipse [14] with two diameters, a shape factor and a principal orientation. The shape factor characterizing the variation in the image geometry, also called coherence factor or dispersion indicator, is obtained from the tensor eigenvalues $\lambda_1(S)$ and $\lambda_2(S)$ by:

$$C(S) = \left(\lambda_1(S) - \lambda_2(S)\right) / \left(\lambda_1(S) + \lambda_2(S)\right), \tag{4}$$

and the main orientation is computed from the eigenvector $e = [e_x, e_y]$ associated with $\lambda_1(S)$ as:

$$O(S) = tan^{-1}\left(e_y / e_x\right), \tag{5}$$

In the sequel, we propose to adapt the WL algorithm [3] to the specificities of tensor-valued images in order to synthesize a structure tensor field similar to the one computed from the sample texture. Therefore, the neighborhood of the output tensor (a vector of tensors) is first captured, then the most similar neighborhood is searched for in the input tensor field, and the corresponding tensor is copied to the target position in the output tensor field. The similarity between two tensors S_1 and S_2 can be measured by means of different tensor-space metrics. In this study, four metrics are considered. In addition to the Euclidian distance (ED) defined in (6), three other metrics are considered: the shape-orientation metric (SO), the Frobenius norm (FN), and the Log-Euclidian metric (LE);

$$M_1(S_1,S_2) = (S_{1xx} - S_{2xx})^2 + (S_{1yy} - S_{2yy})^2 + 2(S_{1xy} - S_{2xy})^2. \tag{6}$$

The SO measures the dissimilarity between tensors in terms of geometric properties (orientation and coherence factors) as in [14]:

$$M_2(S_1,S_2) = M_{or}(S_1,S_2)^{\alpha} \cdot M_{coh}(S_1,S_2)^{1-\alpha}, \tag{7}$$

where α is a weight ranging from 0 to 1, M_{or} is the orientation dissimilarity measure computed as:

$$M_{or} = \left|\sin\left(O(S_1) - O(S_2)\right)\right| \cdot \min\left(C(S_1), C(S_2)\right), \tag{8}$$

and M_{coh} is the coherence dissimilarity measure:

$$M_{coh} = \max\left(\frac{C(S_1)}{C(S_2)}, \frac{C(S_2)}{C(S_1)}\right), \tag{9}$$

The FN metric [14] is given by:

$$M_3(S_1,S_2) = \left[trace\left(\left[S_1 - S_2\right]^T \left[S_1 - S_2\right]\right)\right]^{1/2}, \tag{10}$$

where T is the matrix transpose operator.

The LE metric, also called Riemannian, is given by [15]:

$$M_4(S_1,S_2) = \left[trace\left(\left[\widehat{S_1} - \widehat{S_2}\right]^T \left[\widehat{S_1} - \widehat{S_2}\right]\right)\right]^{1/2}, \tag{11}$$

where $\widehat{S}$ is the matrix logarithm of S.

Two tensor neighborhoods F_1 and F_2 can be compared by computing the sum of their tensor dissimilarity (STD) values as:

$$STD(F_1,F_2) = \sum_{n=1}^{N} M_i\left(F_1(n), F_2(n)\right); \; i \in \{1,2,3,4\}, \tag{12}$$

where N is the number of tensors within each neighborhood and $F(n)$ represents the n-th tensor within the tensor neighborhood F.

One of the most important tasks in the tensor synthesis process is the choice of the tensor neighborhood size and shape, and the adequate scan type, which directly influence the resulting synthesized tensor image. In this paper, we either use a causal neighborhood with a lexicographical scan type (Fig.1.a – left column), or a square non-causal neighborhood with a completely random walk (Fig.1.a – right column). In the first case, the synthesis of a tensor-valued pixel is totally dependent on previous tensors and may lead to a high degree of regularity of the synthesized tensor image (as shown in [1]). On the contrary, in the second case, the random walk allows the synthesized tensor to free itself from its past and may thus multiply the possible configurations.

The neighborhood size has to be adequately chosen in order to preserve texture structures. In order to avoid the use of large neighborhoods which grows the computational cost, a multi-resolution tensor pyramid is used to capture the structures by fewer tensors in higher pyramid levels (smaller resolution). Gaussian pyramids [15, 16] are used for the multi-resolution approach; a pyramid is obtained by smoothing the tensor field with a Gaussian kernel then down-sampling with a 2:1 factor for each additional scale. Pyramid decomposition is applied to the input as well as the output tensor fields. The synthesis starts from the highest pyramid level and ends at the

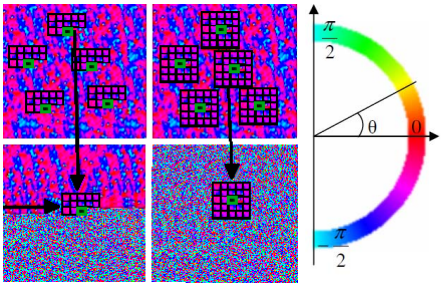

Figure 1. a. L-shaped causal neighborhood adapted to the lexicographical path (left column) and square non-causal neighborhood used with a random walk (right column). **b.** Palette for the orientation field of the structure tensor in (a).

bottom of the pyramid. To assure that the added high-frequency details are consistent with the already synthesized low-frequency structures, the multi-resolution neighborhood of the current tensor at level L contains its same-level neighborhood as well as the neighborhood of the corresponding tensor position at the previously synthesized level (L+1) [3].

3. STRUCTURE TENSOR MAP-CONSTRAINED TEXTURE SYNTHESIS

As mentioned earlier, prior synthesis of a geometric layer may help in the synthesis of the texture layer. Therefore, in our proposed algorithm, the synthesized structure tensor field will be used as a constraint for the texture synthesis. The algorithm takes as inputs the exemplar, its structure tensor field, and the synthesized structure tensor field. The synthesis principle remains the same as the original WL algorithm: for every pixel in the output texture, find in the input texture the pixel with the most similar neighborhood and copy it to the target output position (Fig.2). However, the neighborhood structure must take into account the synthesized structure tensor field. Thus, each neighborhood has two components: a pixel domain neighborhood in the texture image, as well as a tensor domain neighborhood in the structure image. The metric used to measure neighborhood resemblance uses the Sum Square Distance (SSD) for the pixel-domain neighborhood component, and the STD defined in (12) for the tensor-domain component, with a different weight assigned to each domain as:

$$D = p \cdot SSD\left(G_{in}, G_{out}\right) + \left(1-p\right) \cdot STD\left(F_{in}, F_{out}\right), \qquad (13)$$

where p is the weight factor ($p \leq 1$), G is the pixel domain neighborhood component in the input (G_{in}) and output (G_{out}) textures, and F represents the tensor domain component in the initial (F_{in}) and synthesized (F_{out}) tensor

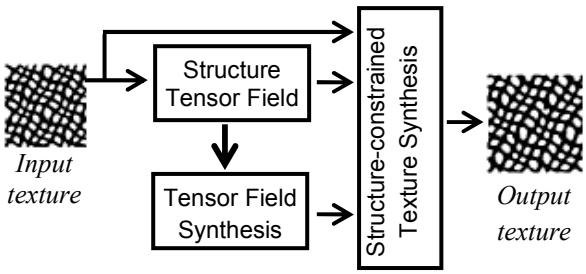

Figure 2. Illustration of the proposed synthesis approach.

fields. The multi-scale extension of the algorithm is straightforward.

4. RESULTS

In this section, the proposed algorithm is evaluated using different input textures from Brodatz database [17] and material samples observed by Transmission Electronic Microscopy. Causal neighborhood with lexicographical scan as well as square non-causal neighborhood with random walk are applied using both the mono-scale and multi-scale synthesis approaches, with the metrics presented in Section 2. Due to space limitations, only a subset of the results is presented. In Fig.3, 4 and 5, the upper row presents (from left to right) the palette used for orientation and coherence images, the input texture and the corresponding structure tensor field represented by its coherence and orientation images, the middle row presents the synthesized structure tensor map represented by its coherence (left) and orientation (right) images, and the bottom row presents the synthesized texture using both the WL (left) and the proposed (right) approaches. In these figures, a causal neighborhood with lexicographical scan is used for the structure and texture synthesis. Table 1 presents the different parameters used for the synthesis.

It can be clearly observed in Fig. 3 and 4 that the proposed approach is able to successfully reproduce the variations of orientations in the exemplar, while the WL algorithm fails. This is due to the additional information provided by the synthesized structure map (tensor field).

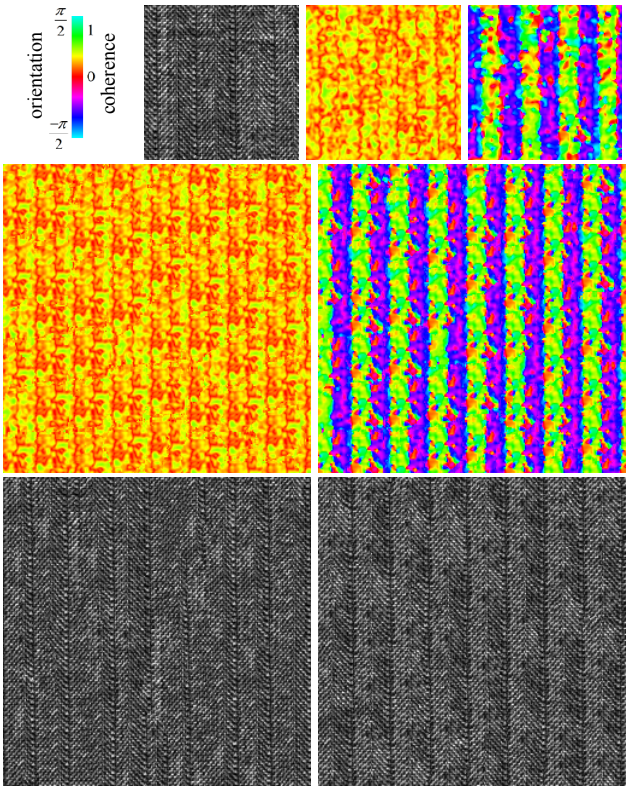

Figure 3. Upper row (from left to right): Used palette, Input texture with its Coherence and Orientation fields. **Middle row**: Coherence (left) and Orientation (right) fields of the synthesized structure tensor field. **Bottom row**: Synthesized texture using the WL (left) and the proposed approach (right).

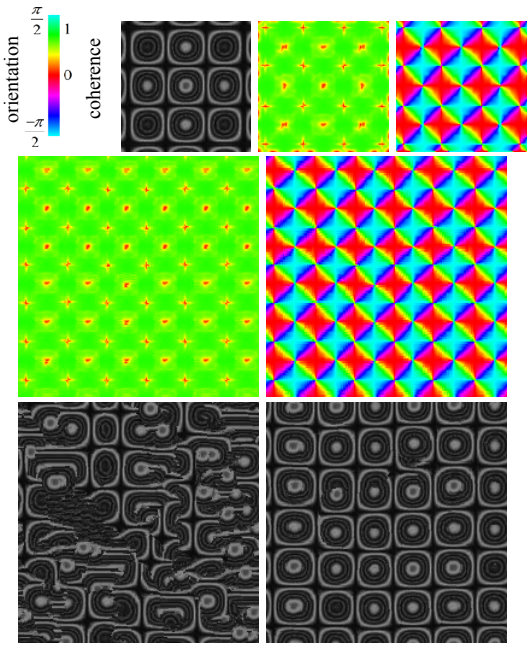

Figure 4. Upper row (from left to right): Used palette, Input texture with its Coherence and Orientation fields. **Middle row**: Coherence (left) and Orientation (right) fields of the synthesized structure tensor field. **Bottom row**: Synthesized texture using the WL (left) and the proposed approach (right).

Fig.5 presents the synthesis result for a material sample showing undulating patterns observed by Transmission Electronic Microscopy. It can be seen that the WL algorithm produces a more regular texture than the exemplar whereas the results obtained by tensor constrained synthesis are more realistic, considering the long range orientation variations of the laminar structures. The proposed algorithm has been evaluated with different scenarios, and our observations are summarized in the sequel. The neighborhood size highly influences the output quality. As the size increases, the output quality improves, at the expense of a higher computational cost. In fact, the appropriate neighborhood size depends on the exemplar, as it must include the texture pattern. Moreover, increasing the number of pyramid levels also improves output quality, since the pyramid decomposition is an alternative to the use of larger neighborhoods. On the other hand, after comparing synthesis results obtained with the various metrics presented in Section 2, we noticed that the influence brought by each metric depends on the input texture. In other words, for some textures, changing the metric does not yield noticeable changes in the synthesized tensor field, and consequently in the synthesized texture, whereas for other textures, an appropriate choice of the metric can result in a better synthesized output. Finally, the synthesis of regular structured textures using the square non causal neighborhood with a random walk requires a larger number of iterations compared to the causal neighborhood with lexicographical scan, for the same output quality. This is expected since the latter depends only on its past which leads to a higher degree of regularity.

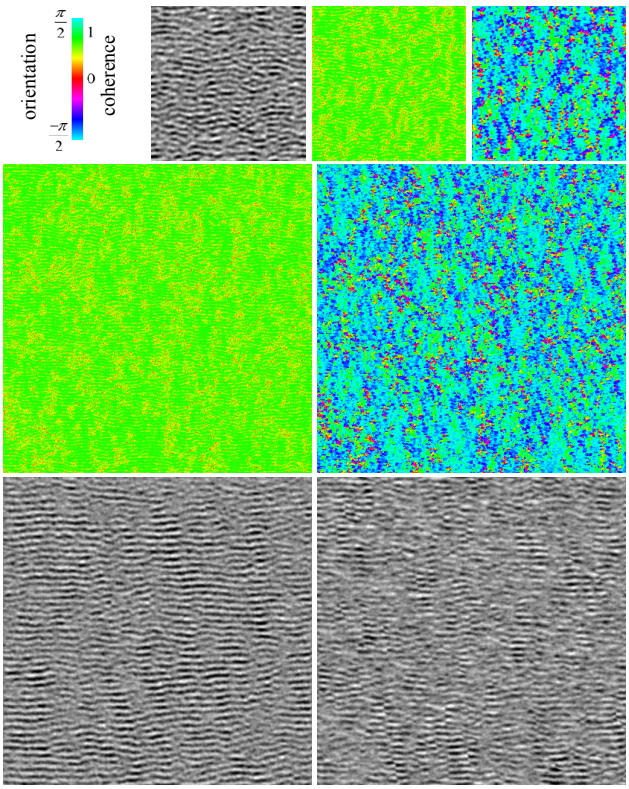

Figure 5. Upper row (from left to right): Used palette, Input texture with its Coherence and Orientation fields. **Middle row**: Coherence (left) and Orientation (right) fields of the synthesized structure tensor field. **Bottom row**: Synthesized texture using the WL (left) and the proposed approach (right).

TABLE I. Parameters used for the synthesis.

Figure :	**3**	**4**	**5**
Input dimensions	128×128	108×108	256×256
Output dimensions	256×256	200×200	512×512
Neighborhood size	13	19	7
Structure pyramid levels	4	3	1
Texture pyramid levels	1	1	1
Tensor dissimilarity	*SO*	*ED*	*ED*
Number of iterations (Structure / Texture)	2/2	3/2	1/1

5. CONCLUSION

Early work on exemplar-based texture synthesis does not deal great with large and multi-scale patterns or with long range directional variations. Therefore, we proposed a two-stage structure/texture synthesis algorithm, where texture synthesis is constrained by a synthesized structure tensor field. Applied on different standard structured textures and composite material samples, the obtained results proved that the proposed method is advantageous for accurately reproducing the exemplar's variations of orientations. As for future perspectives, objective measures have to be developed besides subjective results evaluation. In addition, we aim at reinforcing the use of the tensor map for the synthesis of material samples showing laminar structures observed by Transmission Electronic Microscopy, as well as non-stationary textures.

6. REFERENCES

[1] R. Urs, J.-P. Da Costa, J.-M. Leyssale, G. Vignoles and C. Germain, "Non-parametric synthesis of laminar volumetric textures from a 2D sample," *Proc. of British Machine Vision Conference*, pp. 54.1-54.11, 2012.

[2] J. Portilla and E.P. Simoncelli, "A Parametric Texture Model based on Joint Statistics of Complex Wavelet Coefficients," *Int'l Journal of Computer Vision,* vol. 40(1), pp. 49-71, Oct. 2000.

[3] L.-Y. Wei and M. Levoy, "Fast texture synthesis using tree-structured vector quantization," *Proc. of ACM SIGGRAPH 2000*, pp. 479-488, 2000.

[4] L.-Y. Wei and M. Levoy, "Texture synthesis from multiple sources," *Proc. of ACM SIGGRAPH Sketches & Applications*, 2003.

[5] R. Paget and I.D. Longstaff, "Texture synthesis via a non causal nonparametric multiscale markov random field," *IEEE Trans. on Image Processing*, vol. 7(6), pp. 925–931, 1998.

[6] V. Kwatra, A. Schödl, I. Essa, G. Turk and A. Bobick, "Graphcut Textures: Image and Video Synthesis Using Graph Cuts," *Proc. of ACM SIGGRAPH*, pp. 277-286, 2003.

[7] J. Kopf, C.W. Fu, D. Cohen-Or, O. Deussenn, D. Lischinski and T.T. Wong, "Solid Texture Synthesis from 2D Exemplars," *Proc. of ACM SIGGRAPH*, vol. 26(3), 2007.

[8] J.-P. Da Costa, and C. Germain, "Synthesis of solid textures based on a 2D example: application to the synthesis of 3D carbon structures observed by transmission electronic microscopy," *Proc. of SPIE, Image Processing: Machine Vision Applications III*, vol. 7538, pp. 10, 2010.

[9] R.D. Urs., "Non-parametric synthesis of volumetric textures from a 2D sample", *PhD Thesis, Univ. Bordeaux I*, Mar. 2013.

[10] J.-M. Leyssale, J.-P. Da Costa, C. Germain, P. Weisbecker and G. Vignoles, "An image guided atomistic reconstruction of pyrolytic carbons," *App Phys Lett.*, vol. 95(23), pp. 231912, 2009.

[11] J.-M. Leyssale, J.-P. Da Costa, C. Germain, P. Weisbecker and G. Vignoles, "Structural features of pyrocarbon atomistic models constructed from transmission electron microscopy images," *Carbon*, vol. 50(12), pp. 4388-4400, 2012.

[12] G. Peyré, "Texture Synthesis with grouplets," *IEEE Trans. on Pattern Analysis and Machine Intelligence*, vol. 32(4), pp. 733-746, 2009.

[13] M. Kass and A. Witkin, "Analyzing oriented patterns," *Computer Vision Graphic Image Processing*, vol.37(3), pp. 362-385, 1987.

[14] V. Toujas, M. Donias and Y. Berthoumieu, "Structure Tensor Field Regularization Based on Geometric Features," *European Signal Processing Conference (EUSIPCO)*, Aug. 2010.

[15] P. Fillard, V. Arsigny, N. Ayache and X. Pennec, "A Riemannian framework for the processing of tensor-valued images," *Fogh Olsen, O., Florack, L.M.J., Kuijper, A. (eds.) DSSCV 2005. LNCS,* vol. 3753, pp. 112–123, 2005.

[16] L. Jacques, L. Duval, C. Chaux, G. Peyré, "A panorama on multiscale geometric representations, intertwining spatial, directional and frequency selectivity," *Signal Processing*, vol. 91(2011), pp. 2699–2730, Elsevier, 2011.

[17] P. Brodatz. A Photographic Album for Artists and Designers. *Dover Ed., New York*, 1966.